Stanford Exploration Project, Report 103, April 27, 2000, pages 123–174

Sub-salt imaging of a 2-D elastic synthetic model, using prestack, split-step, wave equation migration

Douglas Gratwick[1]

ABSTRACT

This paper explores methods to image complex structures under a salt body, using a 2-D elastic synthetic model. The modeling algorithm handles complex features such as energy from multiple reflections and mode conversion. I show that a complex wave equation depth migration algorithm is needed to position the salt boundaries and reflectors from sediments below the salt properly. Also, using simple ray-tracing diagrams, I show that energy from converted waves is useful in imaging steeply dipping reflectors below the salt. Though these techniques improve overall image quality, parts of the image under the salt are still left unresolved, and I outline possible techniques for imaging these reflectors.

INTRODUCTION

The use of synthetic models is invaluable in our attempt to better process reflection seismic data (Audebert et al., 1994). The obvious benefit of these models is, of course, that they immediately provide the answer to the underlying question: What is under the surface where the survey is being done? Since the answer is known, individual problems can be isolated. Thus, if the project focus is on testing prestack migration and a synthetic model is used, the known velocity function is exactly correct. On the other hand, if the prestack migration algorithm works, then velocity functions can be modified to find how bad the input velocity function can be before the image is severely distorted (Etgen, 1990; van Trier, 1990; Biondi, 1990).

In this paper, only the prestack migration algorithm will be analyzed. Specifically, problems encountered with the imaging, and some techniques for solving those problems, will be covered. The model used for this project is complex, and thus provides for many interesting imaging problems. It will be shown that for such a complex setting, simple zero-offset migration techniques are not effective, and that more complex migration techniques which account for lateral velocity variations and depth conversion are necessary for a good image. In addition, the paper will demonstrate that even this sophisticated migration algorithm cannot take care of all imaging problems, and that other techniques need to be used in conjunction with the prestack migration algorithm. Specifically, a technique of changing the input velocity function will be implemented. By changing the input velocity of the salt from P-wave to S-wave,

[1]**email:** doug@sep.stanford.edu

reflections from this wavefield are stacked in the image.

2-D SYNTHETIC MODEL

The data used in this project was provided by BP-Amoco, and is a 2-D, fully elastic synthetic model which has a number of complex features that can inhibit good imaging when using conventional methodology. In Figure 1, the P-wave velocity function is shown. The most dominant feature is the large salt body, which stretches for almost 50,000 feet, starting at 15,000 feet. It thickens to a maximum depth of over 3,000 feet. The salt is faulted on the base, and underlying the salt are a series of faulted blocks. Two layers can be seen in the fault blocks, with the layers being anomalously low velocity layers to the right, and slightly high velocity layers to the left. The high velocity layers become more contrasted towards the left of the model. The low velocity layers remain highly contrasted to the right edge of the model.

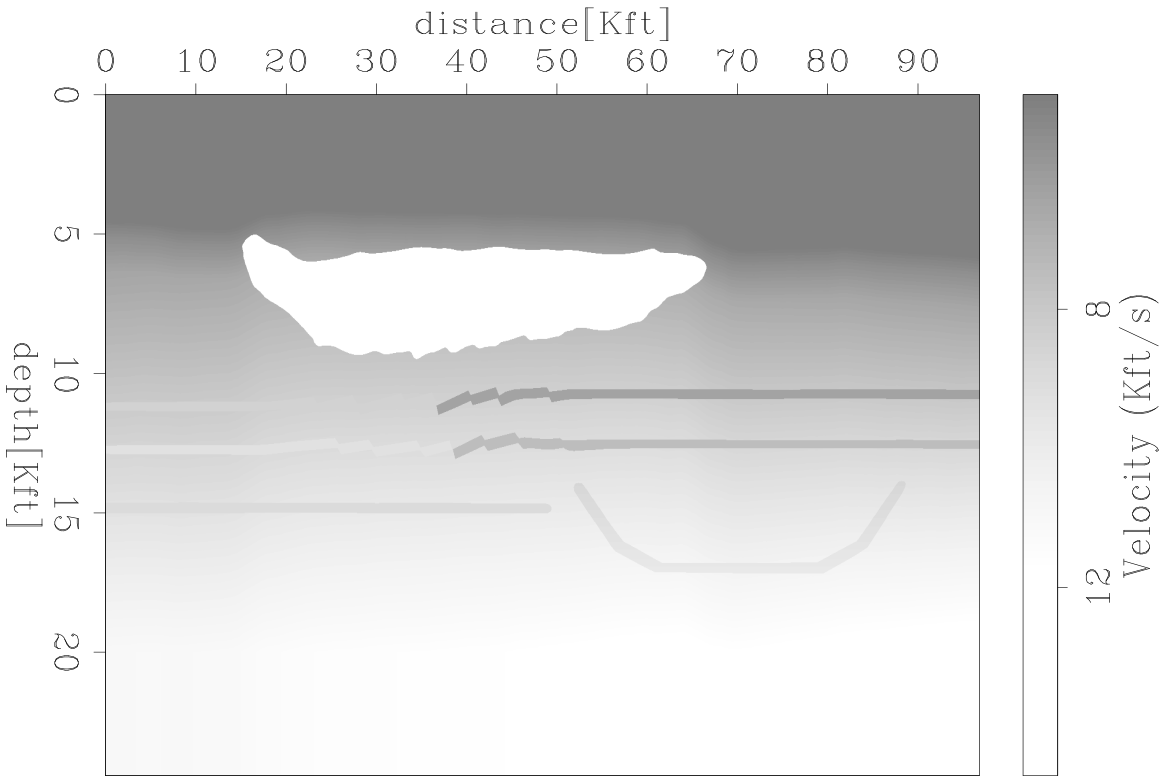

Figure 1: P-Wave Velocity Model doug1-v_p [ER]

Also shown is a synclinal structure (represents a paleochannel) below the two layers mentioned above, as well as a flat lens of sediment which starts on the left edge and stops abruptly underneath the salt. Both the syncline and lens are relatively low velocity layers. The S-wave velocity model seen in Figure 2 shows the same features, except that all the layers are consistently high velocity layers, and the layers in the faulted blocks remain at a constant velocity instead of abruptly changing as in the P-wave model.

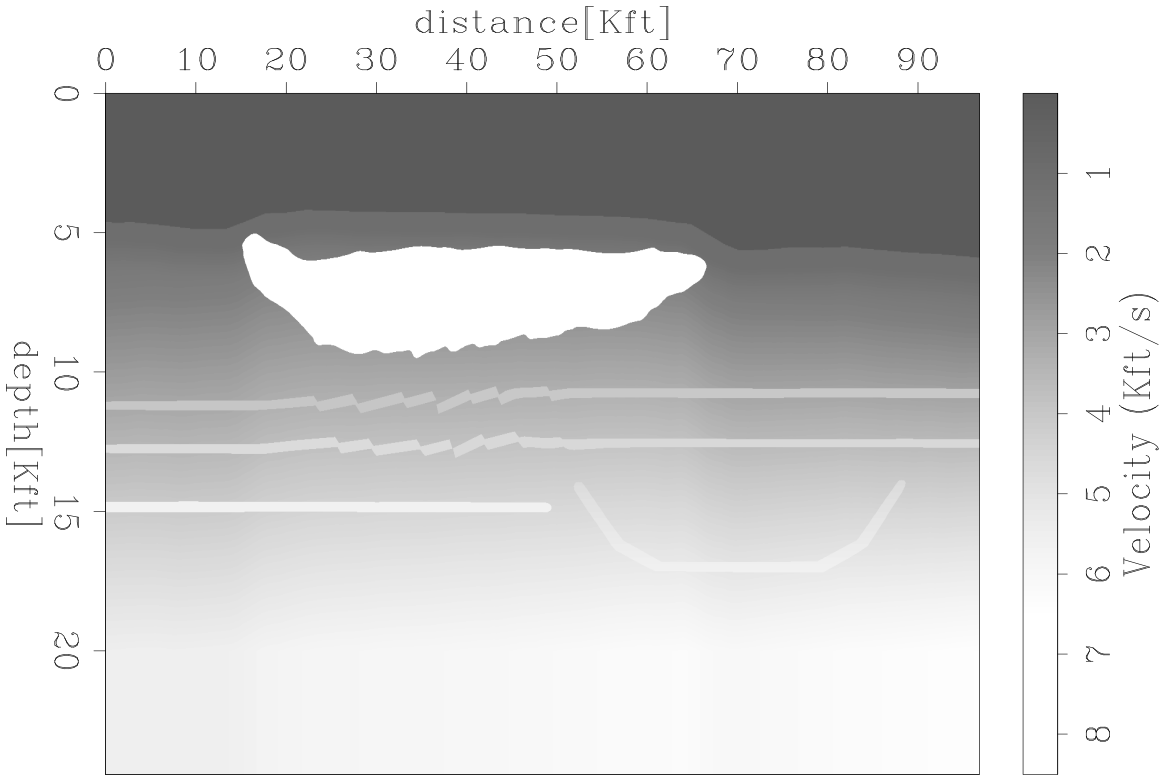

Figure 2: S-Wave Velocity Model doug1-v_s [ER]

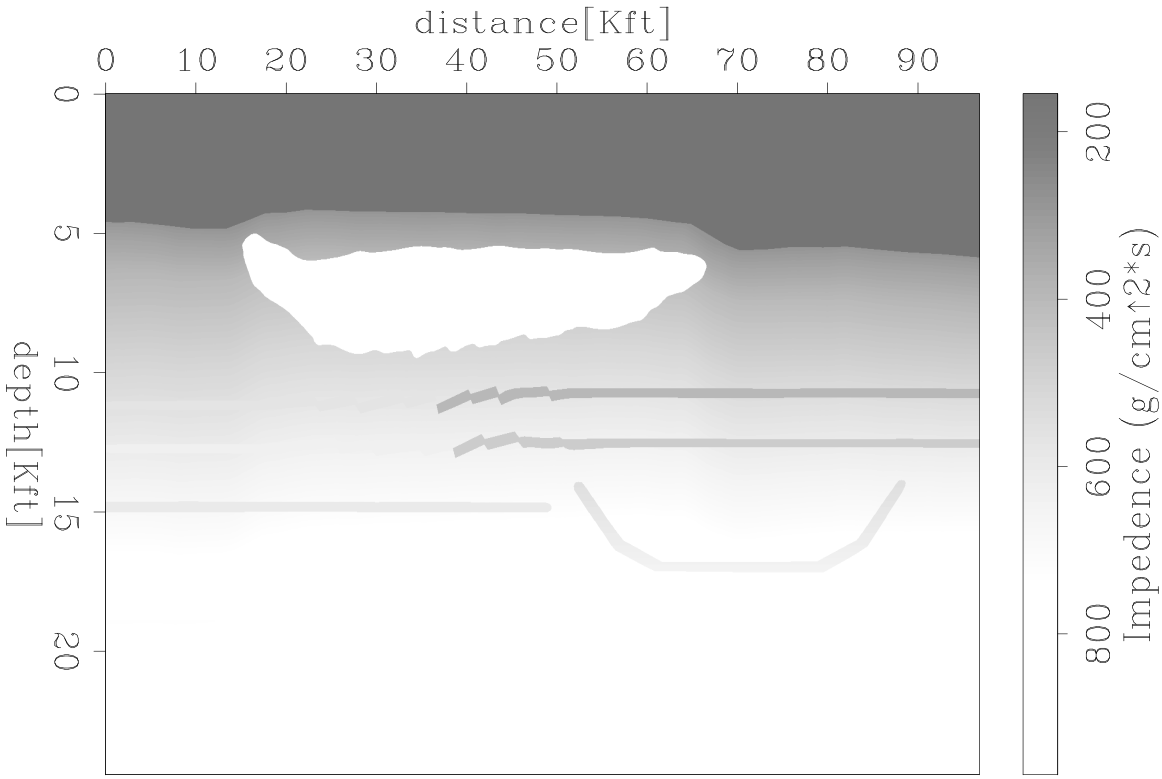

Figure 3: P-Wave Impedance Model doug1-ip_bar [ER]

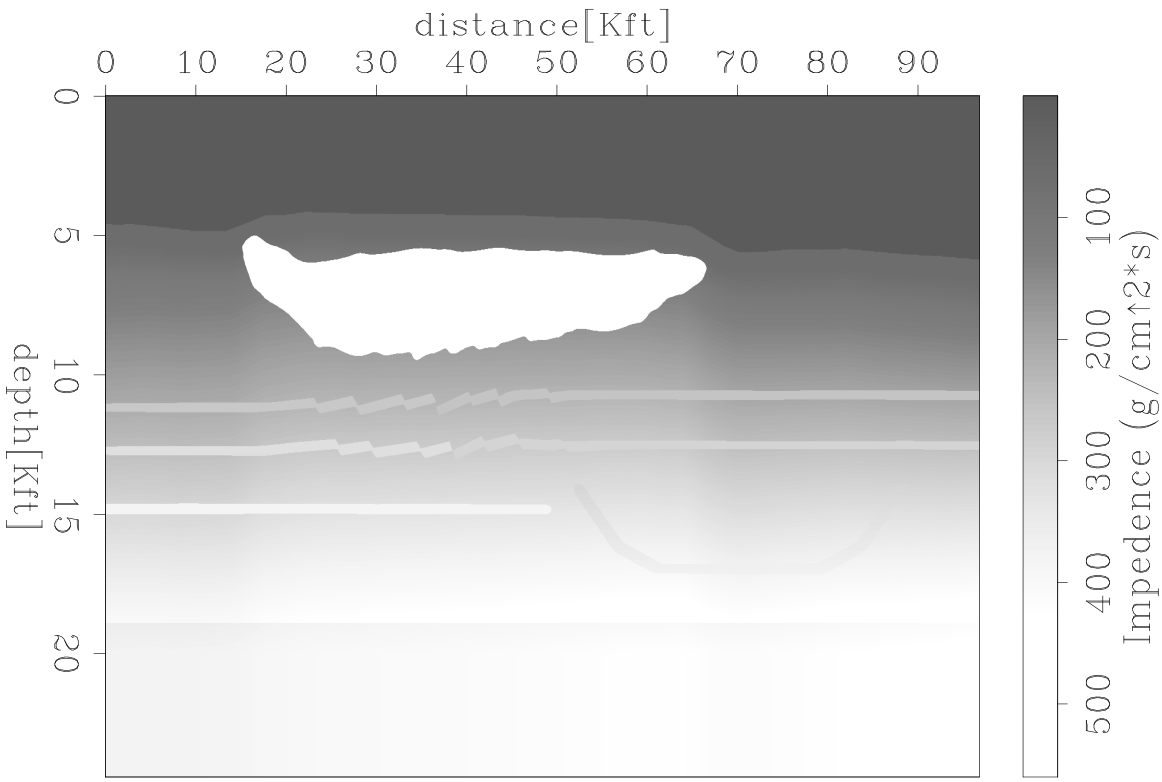

Figure 4: S-Wave Impedance Model doug1-is_bar [ER]

Impedances for the two models are shown in Figures 3 and 4. In the P-wave impedance model, large contrasts are seen for all of the features noted above, with the exception of the two slightly higher velocity layers seen at the left of the model, which end under the salt. In the S-wave impedance model, the impedance contrast remains constant for the two layers. A formula for reflectivity that is based on impedances is

$$R = \frac{Z_2 - Z_1}{Z_1 + Z_2} \tag{1}$$

where R is the reflectivity, and Z_1 and Z_2 are the impedances of the two layers.

From the formula, we can see that the magnitude of the reflection is independent of the position of the layers relative to each other. Rather, it is the sign which changes. So for high impedance over low, the reflection is in the same phase, while for low impedance over high, there is a 180^0 phase shift (Scheriff and Geldart, 1995). For the purposes of imaging, the strength of the reflection becomes important, simply because stronger reflection coefficients mean that the layers will have higher amplitudes in the image. Referring back to Figures 3 and 4, we can see that P-wave energy should be strong from the top and bottom of the salt, as well as from all the other layers, with the exception of the two high velocity layers. However, these layers show a higher S-wave impedance contrast, and thus S-wave energy should be reflected relatively well.

MIGRATION ALGORITHM

The migration algorithm used for this project uses a variation of the split-step Fourier domain migration method, developed by Stoffa (Stoffa et al., 1990). Simple Fourier domain migration based on the single square root operator (SSR) is also known as phase-shift migration (Gazdag, 1978). In phase-shift migration, a wavefield at the surface is downward-continued, assuming the wavefield is generated by the subsurface reflectors exploding (Claerbout and Black, 1997). The single square root operator marches the wavefield down, by shifting in the $\omega - k_x$ domain:

$$e^{ik_z \Delta z} = e^{-i\frac{2\omega}{v}\sqrt{1-\frac{v^2 k_x^2}{4\omega^2}}\Delta z} \tag{2}$$

The imaging principal sums over all ω, giving the wavefield at t=0, which is the migrated image (Yilmaz, 1987). The split-step methods developed by Stoffa use an approximation of the SSR, where v is replaced by an average velocity of a given depth step, v_{ref}. A new term is added to correct for the difference of the average velocity and the actual medium velocity v_m. The equation looks like this variation of equation (2) (k_z is shown):

$$k_z = \sqrt{\frac{4\omega^2}{v_{ref}^2} - k_x^2} + \left(\frac{2\omega}{v_m} - \frac{2\omega}{v_{ref}}\right) \tag{3}$$

In equation (3), the first term is calculated in the $\omega - k_x$ domain, the second in the $\omega - x$ domain. So at every depth step, a 2-D FFT transforms the wavefield into $\omega - k_x$ space. The wavefield is downward-propagated using the phase-shift operator and v=v_{ref}. A 1-D IFFT transforms into $\omega - x$ space, where the correction term is applied. Once again, summing over all frequency gives the image. This method is exact if $v_{ref} = v_m$, or if layers are flat. If lateral velocity variations are significant or units are dipping steeply, a better approximation of the SSR equation is needed. To handle these conditions, we use the double square root equation (DSR). The DSR equation is a higher order approximation of the SSR equation. The DSR equation as displayed in IEI (Claerbout, 1984) is

$$\frac{dU}{dz} = -\frac{i\omega}{v}\left[\sqrt{1-(Y+H)} + \sqrt{1-(Y-H)}\right]U \tag{4}$$

where,

$$Y = \frac{v^2 {K_y}^2}{4\omega^2} \tag{5}$$

and

$$H = \frac{v^2 {K_h}^2}{4\omega^2} \tag{6}$$

The DSR equation inherently includes both migration and NMO. Therefore, with input CMPs and a velocity function, a good image is created. The actual migration program used in

this project is one developed by Biondo Biondi that uses a variation of the split-step method with the DSR equation (Biondi, 1998). The DSR equation can better handle lateral velocity variations as well as steeper dips (as compared to the SSR equation). The use of the split-step method with the DSR makes the algorithm more effective. In this way, multiple reference velocities can be used, and sharp lateral velocity variations, such as salt in contact with sediment, can be handled. For this project, three reference velocities were used. Biondi's program also has an input salt velocity, so that the reference velocities in the sediment will not be anomalously high if the salt is at the same depth step. So for each depth step, three wavefields were generated, then an interpolation in the space domain was used as needed.

ZERO-OFFSET MIGRATION

The main problem with the complex Fourier migration algorithm described above is that it is computationally expensive. However, by looking at the zero-offset section in Figure 5, we see that simple poststack migration will not be satisfactory. Since the salt body is present, a depth migration will help to restore the salt to its correct thickness. Also, with a more complex velocity function, there is a better chance of stacking out a majority of the multiple energy, which is very dominant in the CMP stack. In poststack migration, the object is to collapse diffractions, steepen dips, and uncross bow ties.

Using a poststack phase-shift operator, we can put the dips of the synclinal structure into the correct position, and the bow ties can be uncrossed. However, that is only a very small part of the image. Moreover, the times of those events are unlikely to be correct, especially under the salt. After migration it is still impossible to see under the salt, where the fault blocks are. Therefore, a complex prestack algorithm, though computationally expensive, becomes necessary in this type of complex geologic setting.

PRESTACK MIGRATION WITH P-WAVE VELOCITY MODEL

Initially, the most logical velocity function to input for prestack migration is that of the P-wave model. The energy which ends up in the gathers is usually dominated by P-waves, mainly because in this case, the source is P-wave and the receivers are in the water. So in order to get S-waves, mode conversions must occur. In fact a number of conversions must occur to get P-Waves which convert to S and then convert back to P. Conversion at interfaces reduces the energy, so after a number of conversions, not much energy is left (Scheriff and Geldart, 1995).

The section produced from the input CMPs and the P-wave velocity function is seen in Figure 6. This is an obvious improvement over the stacked section in Figure 5. The salt boundary has been imaged very well, including the faults at the base of the salt. Under the salt, the fault blocks to the right are imaged very well, with the two layers seen in the impedance plots very apparent in the image. However, as expected, the blocks and layers to the left are not very well imaged, because the impedance contrasts are such that not much energy is reflected.

We can also see that the part of the synclinal structure under the salt is not visible. The

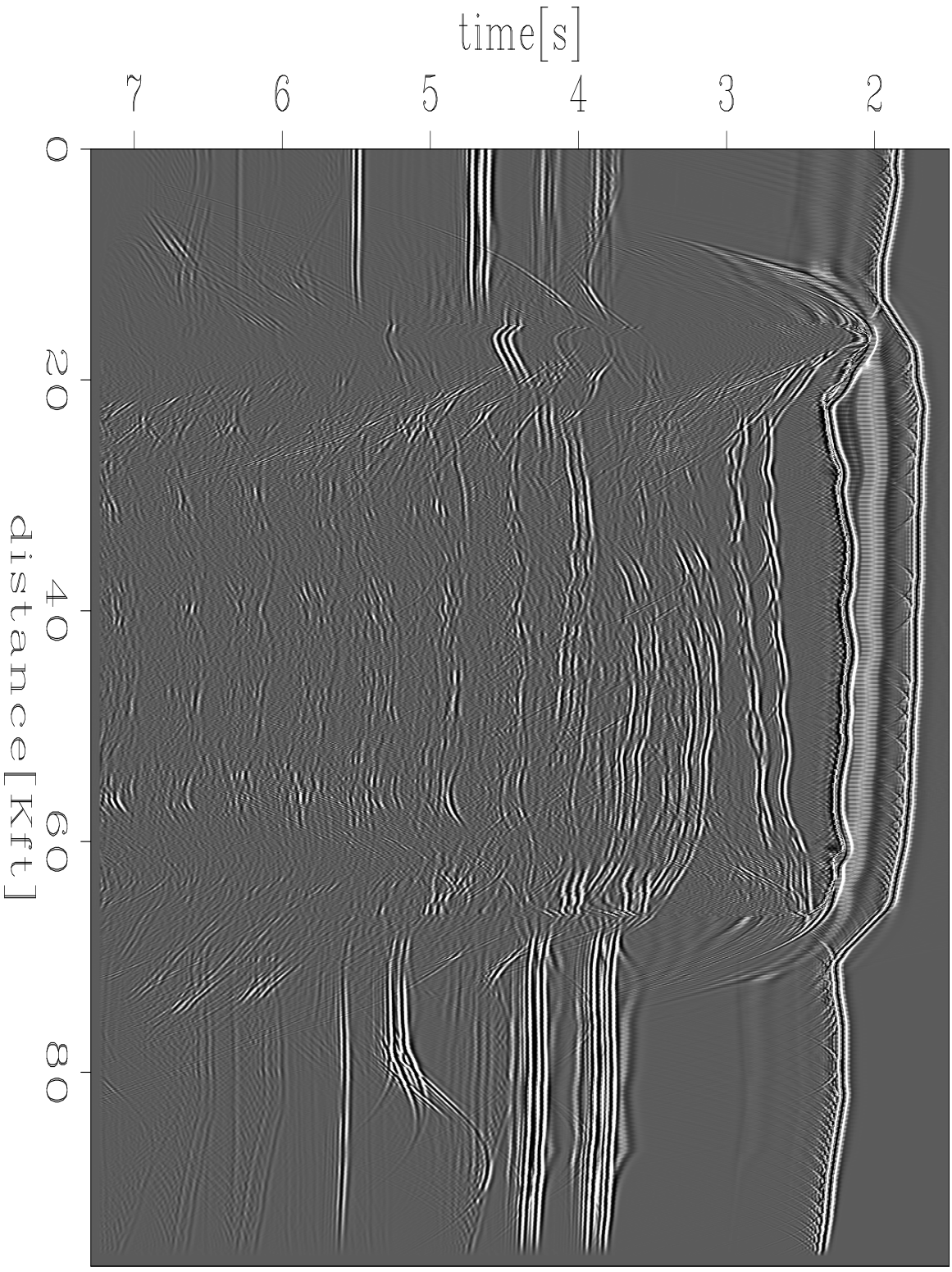

Figure 5: Zero-Offset Section doug1-stack [CR]

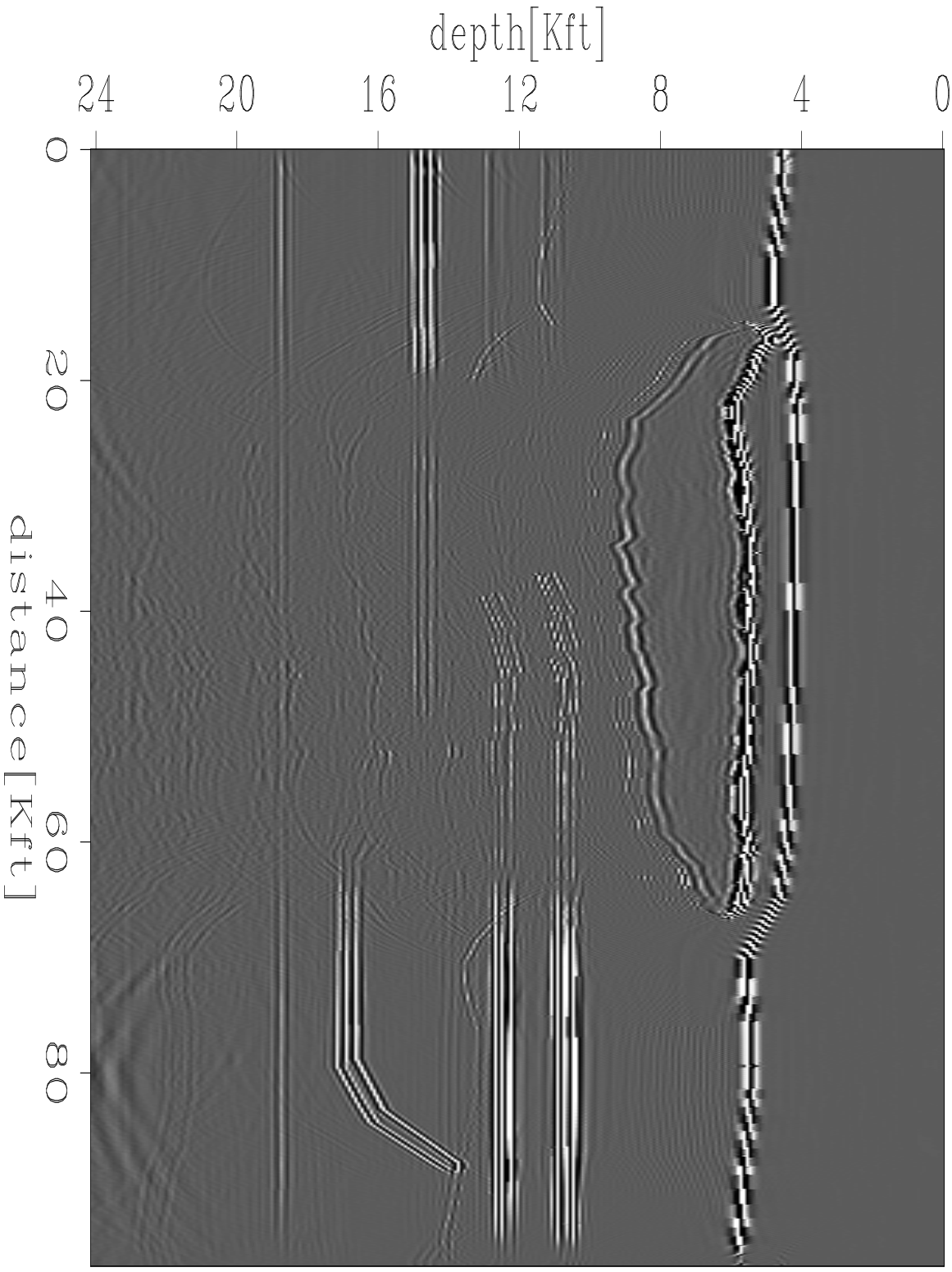

Figure 6: Prestack Migrated Section Using P-Wave Velocity Function doug1-prestack.p [CR]

dips and positions of the right flank seem good, but under the salt, the image is lost. This is likely due to a problem with the raypaths being distorted as the wavefield is going through the salt. This causes less energy to get to the receivers, and thus that part of the image does not show up (Muerdter et al., 1996). The same scattering effects are seen in the lens, which has a shadow zone under the salt boundary where the wavefield energy does not reach the receivers. Another feature is the trace of the salt bottom which appears just a little bit down from the bottom of the salt. This is actually the S-wave energy from the travel of converted waves in the salt which stacks at that velocity. With the exception of these shadow zone problems, and some of the S-wave energy, the image is very good when compared to the actual model.

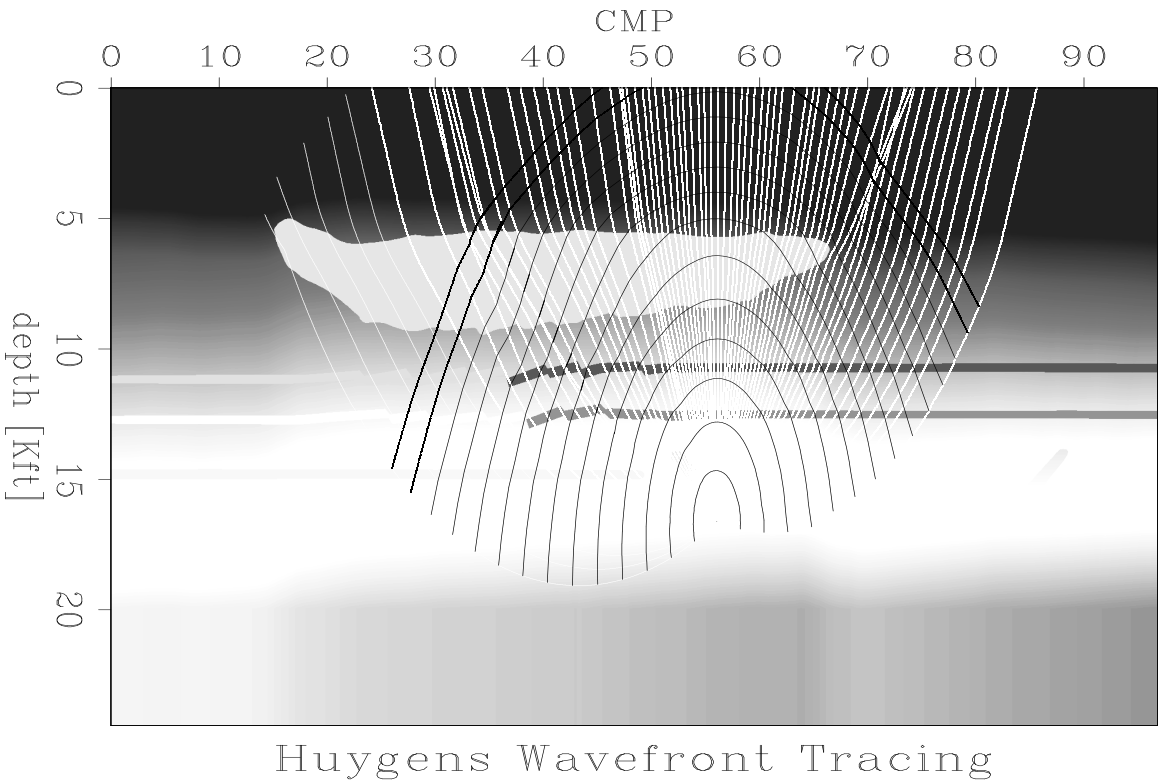

Figure 7: Wavefield Trace Of P-Wave Model With S-Wave Salt Velocity doug1-vwp.saltlow [ER]

PRESTACK MIGRATION WITH MODE-CONVERTED VELOCITY MODEL

Note that the scattering effects of the salt cause much of the P-wave energy to be lost when we are dealing with structures under the edge of the salt body. Moreover, when we consider the steep dip of the synclinal structure, it is no surprise that very little P-wave energy gets to the surface from these areas. The next step is then to change the velocity model to stack different arrivals that have a better chance to make it to the surface (Kessinger, 1996). These arrivals are the ones that are from the wavefield that converts to S-wave through the salt. The interface of the sediment and salt is such that much of converted energy can be produced from an incident

P-wave. Figure 7 shows a ray trace of a wavefield generated on the left flank of the synclinal structure. Note that the wavefield does not scatter through the salt body, which has the S-wave salt velocity, while the sediment has the P-wave velocity.

In the migration that used this new velocity model, we can see that enough of this converted wave energy gets to the receivers that the left flank of the synclinal structure is imaged. Although its amplitude is not very strong, it is enough that an interpreter would recognize the feature. Note also that the trace below the salt bottom that was seen in the previous migrated image has moved to its correct subsurface position (Figure 8). Still not imaged well, however, are the leftmost fault blocks under the salt body, as well as the shadow zone of the lens described in the previous section.

CONCLUSIONS/FUTURE CONSIDERATIONS

It is clear that the migration algorithm described and implemented in this paper does a good job of imaging in the presence of complex geology. The result from the prestack migration vs. the poststack migration shows that in this case, the use of the prestack migration algorithm was not only beneficial, it was necessary. However, the limitations of the use of this procedure by itself are shown in its failure to image certain parts of the model. Though simple tweaking of the velocity model can prove to help image different parts, others were not visible. The faulted blocks with the relatively high S-wave impedance contrasts are symbolic of a real life possibility where the layers are brine-bearing sediments. In this case, these layers are important things to image, so that they are avoided while drilling. To image these parts,we would need some special processing to take place. One method that could be used is multiple attenuation. If the multiples from the water bottom and salt were adequately attenuated, the gain could be turned up and the low amplitude signals might be more easily seen. Another method is to mute the energy in the data so that only the target reflections (deeper units of interest) would be imaged.

Currently, we are considering the latter, and there is initial evidence that the S-wave energy from the left fault block layers is enough that it can be identified and separated from the rest of the energy on the CMP gathers. If this can be done for all the CMPs which correspond to that part of the image, there is a good possibility that we could image these blocks.

REFERENCES

Audebert, F., Biondi, B., Lumley, D., Nichols, D., Rekdal, T., and Urdaneta, H., 1994, Marmousi traveltime computation and imaging comparisons: SEP–**80**, 47–66.

Biondi, B., 1990, Velocity analysis using beam stacks: Ph.D. thesis, Stanford University.

Biondi, B., 1998, 3-D seismic imaging: SEP–**98**, 1–204.

Claerbout, J. F., and Black, J. L., 1997, Basic Earth Imaging: Class notes, http://sepwww.stanford.edu/sep/prof/index.html.

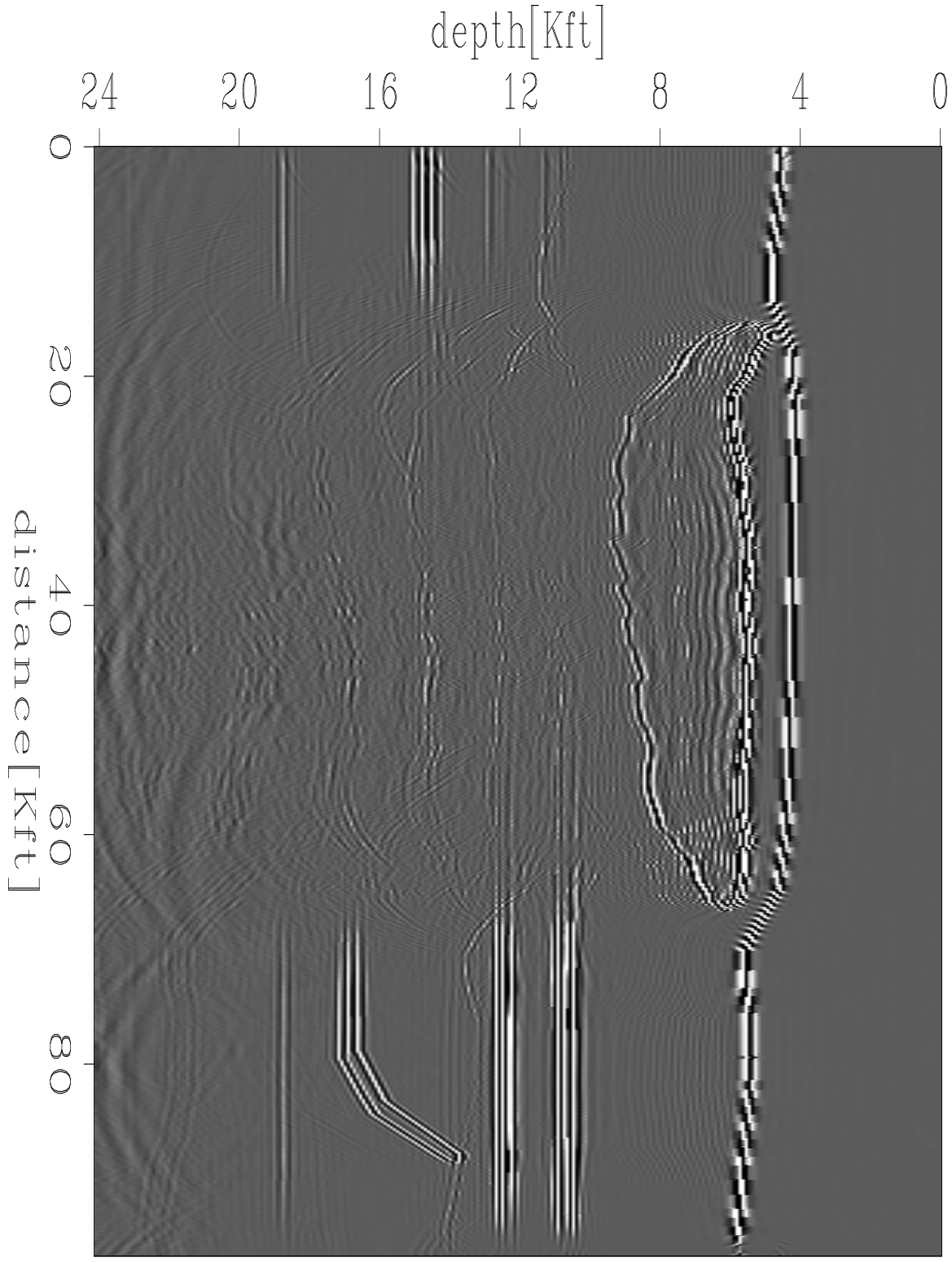

Figure 8: Prestack Migrated Section Using P-Wave Velocity Model with Lowered Salt Velocity doug1-prestack.p.saltlow [CR]

Claerbout, J. F., 1984, Imaging the Earth's Interior: SEP–**40**.

Etgen, J., 1990, Residual prestack migration and interval velocity estimation: Ph.D. thesis, Stanford University.

Gazdag, J., 1978, Wave-equation migration by phase shift: Geophysics, **43**, 1342–1351.

Kessinger, W. e. a., 1996, Subsalt imaging using mode converted energy and acoustic depth migration: 66th Annual Internat. Mtg., Soc. Expl. Geophys., Expanded Abstracts with Authors, v.1 566–569.

Muerdter, D. R., Lindsay, R. O., and Ratcliff, D. W., 1996, Imaging under the edges of salt sheets: a raytracing study: 66th Annual Internat. Mtg., Soc. Expl. Geophys., Expanded Abstracts, 578–580.

Scheriff, R., and Geldart, L., 1995, Exploration seismology: Cambridge.

Stoffa, P., Fokkema, J., de Luna Freire, R. M., and Kessinger, W. P., 1990, Split-step fourier migration: Geophysics, **55 no.4**, 410–421.

van Trier, J., 1990, Tomographic determination of structural velocities from depth migrated seismic data: Ph.D. thesis, Stanford University.

Yilmaz, O., 1987, Seismic data processing: Soc. Expl. Geophys.